Identification of a Thrombin-Binding Region in the Sixth Epidermal Growth Factor-like Repeat of Human Thrombomodulin†

Dmitri Tolkatchev, Andy Ng, Betty Zhu, and Feng Ni*

Biomolecular NMR Laboratory and Montreal Joint Centre for Structural Biology, Biotechnology Research Institute, National Research Council of Canada, 6100 Royalmount Avenue, Montreal, Quebec, Canada H4P 2R2

Received March 29, 2000; Revised Manuscript Received May 16, 2000

ABSTRACT: The interaction of thrombin with a 28-residue peptide corresponding to the N-terminal subdomain of the sixth EGF-like repeat of human thrombomodulin plus the junction between the fifth and the sixth EGF-like domains was characterized in solution by use of NMR spectroscopy, particularly differential resonance perturbations and transferred nuclear Overhauser effects (transferred NOEs). The EGF-like thrombomodulin fragment, or hTM422−449, is conformationally flexible in the absence of thrombin. Upon addition of thrombin, differential resonance perturbations and transferred NOEs are observed for the thrombomodulin peptide, suggesting specific and rapidly reversible binding and structuring of hTM422−449 in complex with thrombin. Residue-specific analysis of the differential line broadening, resonance shifts, and transferred NOEs identified regions of hTM422−449 responding to thrombin binding as the N-terminal residues Thr422−Ile424 and residues His438−Ile447 corresponding to the central β-hairpin, or B-loop, of the consensus EGF-like repeat. The formation of the β-hairpin is supported by the pattern of transferred NOEs bringing the two β-strands together and characterizing a type I β-turn. Docking of the thrombomodulin peptide to the anion-binding exosite I of thrombin revealed structural details capturing binding contacts identified so far as essential for the thrombin−thrombomodulin interaction. Definition of specific interactions between thrombin and a minimal fragment of the sixth EGF-like domain of human TM may lead to the discovery of new peptidomimetic molecules as modulators of blood coagulation.

The epidermal growth factor (EGF)[1]-like protein repeats are found in a large number of proteins including cell surface receptors and components of the blood coagulation cascade (*1*, *2*). These protein modules are believed to play important roles mediating specific protein−protein interactions (*1*, *2*). The EGF-like domains are 40−50 amino acid residues long with limited sequence homology except for the three disulfide bonds defining the characteristic EGF-like fold (*2*). As a rule, the first, or the [1−3], disulfide bond is formed between the first and the third cysteines. The second, or the [2−4], disulfide bond is formed between the second and the fourth cysteines, and the fifth cysteine is connected with the sixth cysteine (the [5−6] disulfide bond). This [1−3, 2−4, 5−6] disulfide connectivity pattern organizes the EGF-like scaffold into two relatively independent subdomains, the N-terminal subdomain, comprising the first two disulfide bonds, and the C-terminal subdomain, reinforced by the third disulfide bond. The N-terminal subdomain consists of two strands of a β-sheet and three loops, packed against the cluster of two crossed disulfide bonds. This structure domain can also be classified as a disulfide β-cross, or T-knot, structural motif, identified in a number of disulfide-rich proteins including the EGF-like repeats, members of other protein growth factors, β-toxins, and plant protease inhibitors (*3*, *4*).

Thrombomodulin (TM) is an important anticoagulant endothelial cell surface protein with six EGF-like repeats in its extracellular region. Thrombomodulin binds to thrombin (IIa) and arrests the interaction of the latter with fibrinogen by blocking IIa's anion-binding exosite I (*5*). The IIa−TM complex also activates protein C, which in turn shuts down the production of IIa by cleaving factors Va and VIIIa (*6*). The cofactor activity of TM has been ascribed to the three EGF-like tandem repeats including the fourth, fifth, and sixth EGF-like domains (TMEGF456) (*7*, *8*). Only the protein fragment including the fifth and sixth EGF-like domains of TM (TMEGF56) appears to be essential for IIa binding (*9*). Alanine scanning mutagenesis (*10*) and binding studies with peptide analogues (*11*, *12*) identified the essential binding region of TM as residues Glu408−Glu426, or the acidic third disulfide loop, of TMEGF5 plus the connecting sequence between TMEGF5 and the sixth EGF-like repeat of TM

† This work was supported in part by the Medical Research Council of Canada (Grant MT-12556) and by the National Research Council of Canada (NRCC Publication No. 42953). A.N. is the recipient of a predoctoral fellowship from the Fonds pour la Formation de Chercheurs et l'Aide à la Recherche (FCAR).

* To whom correspondence should be addressed.

[1] Abbreviations: TM, thrombomodulin; IIa, thrombin; EGF, epidermal growth factor; TMEGF4, the fourth EGF-like domain of thrombomodulin; TMEGF5, the fifth EGF-like domain of thrombomodulin; TMEGF6, the sixth EGF-like domain of thrombomodulin; TMEGF56, the tandem of the fifth and the sixth EGF-like domains of thrombomodulin; TMEGF456, the tandem of the fourth, fifth, and sixth EGF-like domains of thrombomodulin; hTM409−426, a cyclic peptide corresponding to the C-loop of the fifth EGF-like domain of thrombomodulin (residues Cys409−Glu426); hTM436−447, a cyclic peptide derived from the B-loop of the sixth EGF-like domain of thrombomodulin (residues Val436−Ile447); hTM422−449, a peptide corresponding to the N-terminal subdomain of the sixth EGF-like domain of thrombomodulin plus the junction between the fifth and the sixth EGF-like domains (residues Thr422−Gly449); Acm, acetamidomethyl.

10.1021/bi000715e CCC: $19.00
Published on Web 08/03/2000

(TMEGF6). These data are consistent with the fact that deletion of TMEGF6 (residues 425−462) increases the K_D for IIa approximately 10-fold whereas deletion of TMEGF5 (residues 388−424) completely abolished the binding and the cofactor activity of TM for thrombin (*11*).

A significant progress has been made recently in establishing the molecular structure of TMEGF456, or minithrombomodulin, and its mode of interaction with IIa. The three-dimensional structures of the fourth (TMEGF4) and fifth (TMEGF5) EGF-like domains were determined by use of NMR (*13*, *14*). The structure of the TMEGF4 domain resembles that of the EGF molecules (*13*). The oxidized TMEGF4 fragment has the [1−3, 2−4, 5−6] disulfide pairing pattern, common for EGF-like domains. The central two-stranded β-sheet is conserved in TMEGF4 despite the differences between TMEGF4 and EGF in the number of amino acids within this β-sheet. The C-terminal loop of TMEGF4 has a five amino acid insertion, leading to a broadened shape that does not superimpose well on the corresponding EGF loop. On the other hand, TMEGF5 has an uncrossed [1−2, 3−4, 5−6] disulfide-pairing pattern, unusual for EGF-like protein repeats (*14*, *15*). The central β-hairpin typical of all known EGF-like structures appears to be lost in TMEGF5, with the strands running in similar directions but somewhat further apart than in a regular β-structure. The three-dimensional structural details of the IIa−TMEGF5 interface were also characterized in crystal (*16*) and in solution (*17*, *18*). The thrombin-bound structure of the cyclic peptide corresponding to the C-loop of TMEGF5, or residues Cys409−Glu426, was shown to adopt a characteristic conformation with a type II β-turn followed by an antiparallel β-sheet (*18*). The unique structure of the bound peptide appears to be dictated by the complementary hydrophobic and electrostatic interactions between the side chains of Ile414, Ile424, Asp417, and Asp423 of the peptide and the side chains of Phe34, Leu65, Tyr76, Ile82, Arg75, and Arg77A (chymotrypsinogen numbering system) of the thrombin molecule (*18*).

In contrast, the structure of TMEGF6 and its role in IIa binding have been paid comparatively little attention so far. The most recent data on IIa inhibition by TM peptide analogues reported by Lougheed et al. (*12*) suggest that the C-terminal loop of TMEGF6 does not participate in thrombin binding, while the N-terminal subdomain may bind thrombin only very weakly. However, it is not yet clear if the binding of the peptides from the N-terminal subdomain of TMEGF6 was specific and if the effect of the sixth EGF-like domain on the binding of TMEGF56 can be explained by direct interaction of TMEGF6 with the thrombin exosite or by modulating the three-dimensional structure and, hence, the affinity of TMEGF5 (*19*). We achieved a further understanding of the role of TMEGF6 in IIa binding by studying the inhibitory properties of two peptides corresponding to residues Thr422−Gly449 of TM, or the N-terminal subdomain of TMEGF6 plus the junction between TMEGF5 and TMEGF6 (*20*). These peptides had the same amino acid sequence but had either the uncrossed [1−2, 3−4] or the crossed [1−3, 2−4] disulfide-pairing patterns. These peptides also contain a consensus sequence for a calcium-binding site (*21*, *22*). Although neither peptide had a well-defined three-dimensional structure in solution, the crossed [1−3, 2−4] isomer showed a better inhibition potency than its uncrossed analogue. The [1−3, 2−4] isomer was also a markedly better calcium binder. These findings imply that TMEGF6 may have a regular [1−3, 2−4, 5−6] disulfide pattern that is required for specific binding with both calcium and IIa.

In this study, we performed NMR experiments to characterize the interaction of thrombin with the [1−3, 2−4] isomer of the Thr422−Gly449 thrombomodulin fragment. Titration of less than stoichiometric amounts of thrombin into the peptide caused differential resonance perturbations and enhancement of nuclear Overhauser effects (NOEs), indicating rapid exchange between the free peptide and the peptide−thrombin complex (*23*). We demonstrate that the binding of thrombin to the thrombomodulin peptide induces structuring of the TM peptide localized at a region corresponding to the central β-hairpin of all EGF-like repeats, thus confirming the direct and specific character of their interaction. These data provide novel information and further understanding of the binding interactions between human thrombomodulin and thrombin.

MATERIALS AND METHODS

Sample Preparation. The synthetic peptides, T_{422}DIDEC-ENG$_{430}$GFC(Acm)SGVCHNL$_{440}$PGTFEC(Acm)ISG$_{449}$[hTM422−449], VCHNL$_{440}$PGTFE$_{445}$CI [hTM436−447], CSHNL$_{440}$-PGTFE$_{445}$SC [hTM436−447(V436C,C437S,C446S,I447C)], CSHNL$_{440}$PGTFE$_{445}$CI [hTM436−447(V436C,C437S)], and VCHNL$_{440}$PGTFC$_{445}$SI [hTM436−447(E445C,C446S)], where C(Acm) stands for an *S*-acetamidomethyl-protected cysteine, were prepared by solid-phase peptide synthesis using standard Fmoc chemistry on an Applied Biosystems 431A peptide synthesizer. Residue Cys448 of the original thrombomodulin sequence was replaced by serine in hTM422−449 to avoid undesirable disulfide coupling. Peptide hTM436−447 and its analogues were oxidized overnight in 1% ammonium acetate buffer, pH 8.5, as described in ref *20*, and purified by HPLC. The criss-cross [1−3, 2−4] disulfide isomer of hTM422−449 was prepared in two oxidation steps and purified as described previously (*20*). Bovine α-thrombin was purified by cation-exchange chromatography from the bovine plasma barium citrate eluate (Sigma), containing primarily prothrombin and minor amounts of factors X, IX, and VII, after controlled activation by the *Echis carinatus* snake venom (Sigma) (*24*). The active site of purified α-thrombin was inhibited by a 2-fold excess of D-Phe-Pro-Arg-CH_2Cl (PPACK) to prevent thrombin autolysis. The inactivated protein was concentrated to 14−32 mg/mL with CentriCon-10 concentration cells (Amicon) and stored in small aliquots at −80 °C until use.

The NMR samples were prepared by dissolving the peptides to a concentration of about 0.5 mM in 20 mM sodium acetate-d_3 buffer, and 10% D_2O, pH 5.5. For one-dimensional proton NMR titration, aliquots of thrombin at a concentration of 14−32 mg/mL were added to the peptide solutions prepared in the same buffer. The thrombin/peptide ratio was 1:10 for transferred NOE experiments.

NMR Spectroscopy. NMR data were collected on Bruker Avance-500 or Avance-800 NMR spectrometers. TOCSY (τ_{SL} = 35−65 ms) spectra (*25*) and NOESY (τ_m = 150−250 ms) spectra (*26*) were obtained at temperatures of 288 and 298 K. The water solvent signal was suppressed using the WATERGATE procedure (*27*). The spin-lock used in

the TOCSY experiments was an MLEV-17 sequence (*28*) with a field strength of 8.3 kHz preceded and followed by a 2.0 ms trim pulse. The collected FID data were processed using the Bruker XWINNMR program. Spectral visualization, analysis, and assignment were carried out manually on plotted spectra and on Silicon Graphics workstations with the program PRONTO (*29*). All proton chemical shifts are referenced to the proton resonance (δ_{DSS}) of internal DSS, which was set to 0.0 ppm.

Structure Calculations. The experimental NOE distances for hTM422−449 were divided into three categories with upper bounds of 2.5, 3.0, and 5.0 Å, based on the intensity of the corresponding cross-peaks. Individual distances were categorized by an approximate calibration against the intensities of the NOE peaks between geminal protons. The number of unique and ambiguous distance constraints totaled 52 and 14, respectively, including those involving prochiral centers treated using the summation procedure (*23*, *30*). A total of 100 initial structures were calculated using the X-PLOR program (*31*) using a standard protocol of distance geometry followed by simulated annealing (DG/SA). The NOE penalty function is a square-well potential with a weight of 50 kcal mol^{-1} $Å^{-2}$ throughout the calculations. A final set of 100 structures was refined with X-PLOR using a simulated annealing protocol. Structure calculations were also carried out using a variable-target function (VTF) protocol, with fixed bond angles and bond lengths as provided in the ECEPP/3 database (*32*−*34*). An initial set of structures was computed by use of distance constraints derived from well-resolved transferred NOEs. This set of initial structures served as a starting point for the subsequent rounds of structure calculations incorporating both unique and ambiguous distance constraints. The calculated structures using X-PLOR and ECEPP/VTF were very similar. Only structures from X-PLOR calculations were retained for subsequent analysis. The Sybyl and InsightII molecular graphics programs were used for structure manipulation and viewing.

Computation of the Thrombin−TMEGF456 Complex. A model of TMEGF456 was built using the thrombin-bound structure of the C-loop region of the fifth EGF-like repeat, or hTM409−426 (*18*), the three-dimensional structures of the fourth and fifth EGF-like domains (*13*, *14*), and a model structure for hTM422−449 constructed on the basis of the consensus folding topology for EGF-like domains (*2*). TMEGF456 thus constructed was docked to the exosite I of thrombin through superposition of the C-loop of TMEGF5 on the structure of the hTM409−426 peptide docked to thrombin (*18*). Steric clashes and unfavorable van der Waals interactions were released through 15 000 steps of Powell energy minimization using the X-PLOR program, incorporating distance constraints for the C-loop of TMEGF5 and for hTM422−449 determined from transferred NOEs. The NOE penalty function is a square-well potential with a weight of 50 kcal mol^{-1} $Å^{-2}$. Nonbonded interactions were calculated only within the ligand and between the TMEGF456 ligand and thrombin. The weight of the van der Waals energy term was 4.0, and the electrostatic interactions were calculated with a weight of 0.5. Positions of the thrombin residues were fixed, and the residues of the C-loop of TMEGF5 were somewhat fixed through distance constraints between the C^{γ} atom of Asp416 and the C^{ζ} atom of Arg67 and between the C^{γ} atom of Glu417 and the C^{ζ} atom of Arg75 of thrombomodulin and thrombin, respectively. The calcium-binding site was incorporated into the model through distance constraints between the functional donor atoms of the coordinating sphere as determined from the X-ray structure of a consensus calcium-binding site (*35*). The maximal distance between the backbone carbonyl oxygen atom of Ile424 and OE1, OE2 of Glu426 was set to 5.5 Å. The maximal distances between the backbone carbonyl oxygen atom of Leu440 and OE1, OE2 of Glu426, between the OD1 of Asn439 and OD1, OD2 of Asp423, and between the OD1 of Asn439 and OE1, OE2 of Glu426 were set to 5.0 Å. The rest of TMEGF456 was allowed to move freely during the energy minimization.

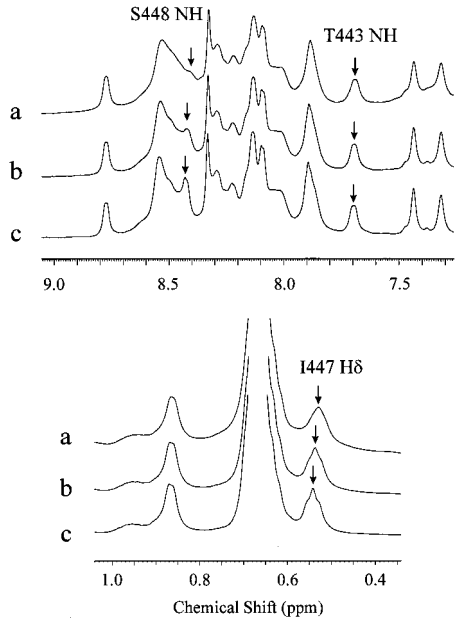

FIGURE 1: Proton NMR spectra of hTM422−449 titrated with thrombin in solution. To 250 μL of 0.5 mM hTM422−449 solution in 20 mM sodium acetate-d_3 buffer, pH 5.5, and 10% D_2O was added (a) 60 μM, (b) 33 μM, or (c) 0 μM PPACK−thrombin stock solution (13.6 mg/mL) in the same buffer. NMR spectra were recorded at 288 K and at 500 MHz.

Theoretical transferred NOEs were calculated for the computed structure of hTM422−449 using the program PDB2NOE (*23*). The tumbling correlation time for the thrombin−peptide complex was set to 20 ns, which is expected for a protein complex with a molecular mass of ~40 kDa. A dissociation constant of 80 μM was estimated on the basis of the peptide concentration, which doubles the clotting time (*20*). The computed NOE intensities were converted into simulated NOESY spectra for comparison with experimental NOESY data sets. The simulated FIDs were calculated by use of experimental chemical shifts determined for all proton resonances of hTM422−449 (*20*) and were transformed into the NOESY spectra using identical processing parameters as the experimental data sets.

RESULTS

Binding-Induced Differential Resonance Perturbation. Upon titration of thrombin into a solution of the hTM422−449 peptide, selected proton resonances of the peptide experienced shifts or line broadening, suggesting a rapid exchange between the free and thrombin-bound states of the peptide. As shown in Figure 1, these broadening effects or resonance shifts can be identified for well-resolved NH

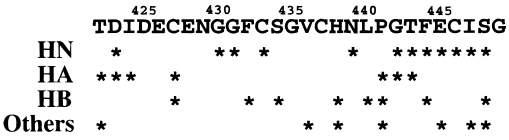

FIGURE 2: Summary of the broadened and/or shifted proton NMR signals in hTM422−449 titrated with thrombin. Asterisks indicate the broadened and/or shifted signals upon addition of 60 μM PPACK−thrombin stock solution (13.6 mg/mL) to hTM422−449. NMR spectra were recorded at 800 MHz. Other experimental conditions were as in Figure 1.

resonances of Ser448 and Thr443 and for the H^{δ} resonance of Ile447. We carried out a detailed analysis of the peptide 1D and 2D spectra obtained at 800 MHz, in the presence and absence of thrombin, and identified additional resonances that displayed broadening or shifts upon thrombin addition. The results are summarized in Figure 2. Major changes in the NH part of the spectrum come from residues spanning the region Asn439−Ser448 of the peptide. Also, the $C^{\delta}H$ protons of Pro441 are significantly affected. Residues Asn439−Ser448 correspond to a double-stranded consensus β-hairpin in EGF-like repeats. On the basis of homology with other EGF-like domains, the β-hairpin in the full-length TMEGF6 presumably spans the loop Val436−Ser448 containing two half-cystines. We also observed some broadening of the NH resonances of the residues Asp423, Gly430, Gly431, and Cys433.

Perturbation of the $C^{\alpha}H$ protons is consistent with changes in the NH region of the peptide NMR spectrum, with residues Thr422−Ile424, Cys427, and Pro441−Thr443 the most affected by the addition of thrombin. The perturbation of the NH and $C^{\alpha}H$ resonances can be ascribed to conformational changes in the peptide and/or direct interaction of the peptide residues with thrombin. The spectral differences in the first three residues of the peptide fragment are in agreement with the results obtained previously (*11*, *12*, *16*−*18*), showing that the first five residues of hTM422−449 directly participate in thrombin binding. Residues Leu440−Phe444 of hTM422−449 correspond to a reverse β-turn linking the two strands of the central β-hairpin, typical of folded EGF-like structures. Therefore, the broadening of the $C^{\alpha}H$ resonances of residues Pro441−Thr443 may indicate the formation of a well-defined reverse β-turn or establishing contacts between these residues and thrombin. Folding of the putative β-hairpin upon binding to thrombin is also indicated by the perturbations of some side-chain resonances including those for residues His438, Pro441, Glu445, Ile447, and Ser448 (Figure 2).

Transferred Nuclear Overhauser Effects. In solution, hTM422−449 displays poor amide and $C^{\alpha}H$ resonance dispersion and shows very few nonsequential NOE connectivities, suggesting the absence of a well-defined three-dimensional structure for the free peptide (*20*). Upon addition of less than stoichiometric amounts of thrombin, we observed selective enhancement of the NOE intensities characteristic of transferred NOEs for the thrombin−peptide complex (*23*). Enhancement of NOEs and differential resonance perturbations show that the N-terminal subdomain of TMEGF6 binds to thrombin selectively, in agreement with binding studies with peptide analogues (*11*, *12*, *20*).

Observation of transferred NOEs in the presence of thrombin suggests that the binding site of thrombin must

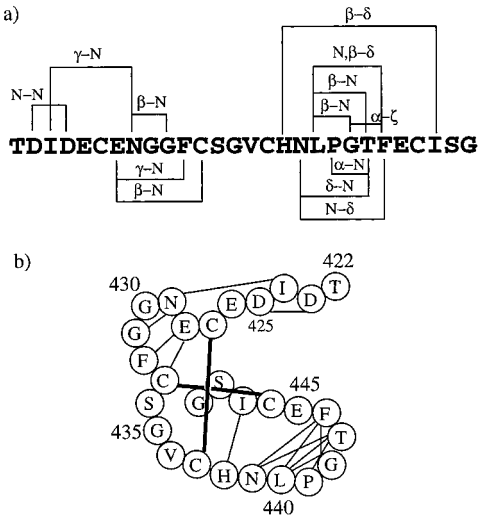

FIGURE 3: Summary of the transferred NOE connectivities (a) for hTM422−449 and spatial organization (b) of the peptide fragment. Hairlines in (b) show the transferred NOE connectivities. The NOESY spectra were collected at 800 MHz.

restrict the conformations of the peptide. Unfortunately, some of the NOE cross-peaks could not be assigned unambiguously because of resonance overlaps. Nevertheless, the thrombin−peptide complex exhibited unique medium- and long-range NOE contacts, demonstrating partial structuring of the peptide fragment upon binding to thrombin (Figure 3). Interestingly, the transferred NOEs were concentrated in the regions marked by significant resonance perturbations (Figures 2 and 3). In the C-terminal half of the peptide unique side-chain to side-chain NOE contacts were present for the proton pairs His438 H^{β}−Ile447 H^{δ}, Leu440 H^{β}−Phe444 $H^{\delta,\zeta}$, and Gly442 H^{α}−Phe444 H^{ζ}. Also, side-chain−NH proton contacts were observed for proton pairs Asn439 H^{δ}−Thr443 NH, Asn439 NH−Phe444 H^{δ}, Leu440 H^{β}−Gly442 NH, Leu440 H^{β}−Thr443 NH, Leu440 NH−Phe444 H^{δ}, and Pro441 H^{α}−Thr443 NH. Some but a smaller number of medium- and long-range transferred NOEs were also observed in the N-terminal half of the peptide. The partial structuring of the N-terminal part of the peptide fragment is also in agreement with the established involvement of these N-terminal residues in direct binding to thrombin (*11*, *12*). In addition, a number of transferred NOEs were observed for residues Glu428−Cys433, indicating partial structuring also for this sequence region. A schematic representation of the chain folding with the observed NOE contacts is shown in Figure 3b. The two strands of the His438−Ile447 stretch are brought together by long-range NOEs between His438 and Ile447, between Asn439 and Phe444, and by a reverse β-turn formed by residues Leu440−Phe444. NOE contacts between Pro441 H^{α} and Thr443 NH, Gly442 NH and Thr443 NH, and Pro441 H^{δ} and Gly442 NH identify a type I β-turn.

The observed transferred NOEs outline the secondary structure elements formed in hTM422−449 upon binding to thrombin. However, the number of experimental NOEs may not be sufficient to calculate a well-defined structure of the bound peptide. Nevertheless, we attempted to carry out a formal structure calculation to obtain a general fold of the peptide. This task is feasible since the presence of the two crossed disulfide bonds markedly restrains the number of possible folds that the peptide can adopt (Figure 3b). The folding of hTM422−449 was calculated using 38 sequential

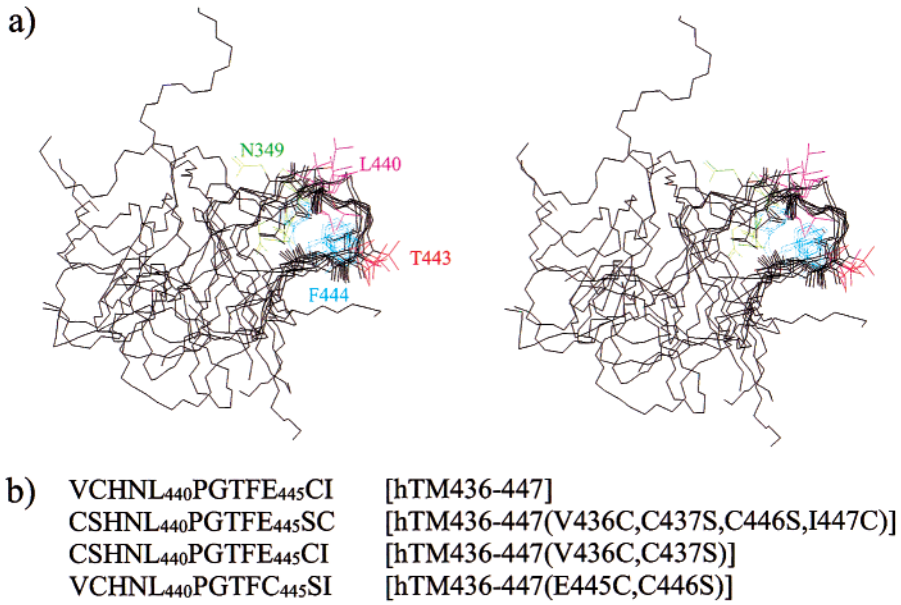

FIGURE 4: A cluster of the nine best structures of hTM422−449 shown in stereoview (a) and the amino acid sequences of analogue cyclic peptides (b) derived from the region Val436−Ile447. The side chains of Asn439, Leu440, Thr443, and Phe444 are shown in color to emphasize their spatial positions. Superposition of all the structures was carried out using the C^{α} atoms of residues His438−Cys446.

and 14 medium- plus long-range unique NOE constraints. Of the 100 calculated structures, 9 of the lowest NOE energy were chosen for further analysis (see Materials and Methods for more details). Indeed, the global fold of the peptide is not well defined by the NOE constraints, as seen by the superposition of the 9 best structures from the calculation (Figure 4a). On the other hand, there is a reasonably defined area in the structure that includes residues Ile424−Phe432 and Cys437−Cys446. In addition, the Cys437−Cys446 region is slightly better defined than Ile424−Phe432, obviously because it contains 33 unique distance constraints out of 52 used in the calculation. The thrombin-bound conformation for residues Cys437−Cys446 indicates the presence of a two-stranded β-hairpin stapled together by a type I β-turn, in agreement with the three-dimensional structure of a consensus EGF-like repeat.

Interaction of Thrombin with Peptides Derived from hTM422−449. On the basis of the obtained NMR information (Figures 2, 3, and 4a), a smaller peptide was derived from the β-hairpin region of hTM422−449, or Val436−Ile447, that may act as a thrombin binder/inhibitor if its conformation is restricted to the same as recognized by thrombin (Figure 4b). We adopted a strategy of cyclization using a disulfide bond in order to limit the conformations available to small peptide fragments (*36*). However, cyclization of the naturally occurring Cys437 and Cys446 may not fully satisfy the steric requirements for the β-hairpin conformation determined for the thrombin-bound hTM422−449, since it would correspond to the [3−4] disulfide bond, which is not present in the natural protein (*20*). In fact, it is the [1−3, 2−4] isomer of hTM422−449 that was shown to have an increased inhibitory potency as compared with the peptide with the unnatural [1−2, 3−4] disulfide pairing (*20*). To explore the possibility of adjusting the disulfide bonding to a desirable β-hairpin, we synthesized four 12-residue analogues derived from the Val436−Ile447 fragment with a varying size of the disulfide loop (Figure 4b) and studied their binding to thrombin by inhibition assays and by use of NMR. The peptides were chosen in such a way, that, when superimposed on the defined β-hairpin of hTM422−449, the side chains of the cysteine residues were in sufficient proximity to form a disulfide bond.

All the cyclic peptides were prepared by an overnight air oxidation of the reduced forms in ammonium acetate buffer, at pH 8.5, at room temperature. Purified cyclic peptides were extensively desalted on C_{18} Sep-Pak columns. To determine inhibitory potency of the peptides, we used a standard clotting assay described in the Materials and Methods. For all of the peptides we did not detect any measurable inhibition of fibrinogen clotting. If the peptides were not sufficiently desalted prior to clotting assays, double clotting time concentrations ranging from 0.5 to 1.2 mM were observed for all of the samples. Hence, thorough desalting of the peptides is necessary to distinguish between weak inhibitory potency and nonspecific salt effects. The absence of inhibition can be explained either by the weak binding or by the lack of interference of the binding of fibrinogen to thrombin by the hTM436−447 series of peptides.

To establish if the TM peptides interact with thrombin, we used NMR to determine differential resonance perturbations induced by thrombin binding. Upon titration of thrombin differential proton resonance perturbations were observed only for hTM436−447, the peptide with the native sequence, suggesting specific binding. There were broadening and/or shifts for the NH resonances of Thr443, Phe444, Cys446, and Ile447 (Figure 5). The NMR spectra of the other three analogue peptides, hTM436−447(V436C,C437S,-C446S,I447C), hTM436−447(V436C,C437S), and hTM436−447(E445C,C446S), did not respond to the thrombin titration (data not shown). Therefore, binding of hTM436−447 to thrombin appears to be sequence specific as well.

Modeling of the Interaction Interface between Thrombin and Thrombomodulin. The observed transferred NOEs within hTM422−449 provide enough information to visualize the local fold of the peptide in complex with thrombin. At the same time, the bound structure and intermolecular contacts

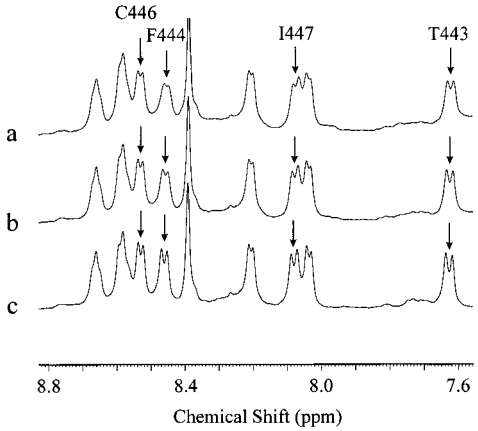

FIGURE 5: Proton NMR spectra of hTM436−447 titrated with thrombin in solution. To 450 μL of 0.5 mM hTM436−447 solution in 20 mM sodium acetate-d_3 buffer, pH 5.5, and 10% D_2O was added (a) 86 μM, (b) 45 μM, or (c) 0 μM PPACK−thrombin stock solution (32 mg/mL) in the same buffer. Proton NMR spectra were recorded at 288 K and at 500 MHz.

of a peptide corresponding to the C-terminal loop of the fifth EGF-like domain of TM, including the first five residues of hTM422−449, have been established and reported previously (*16*, *18*). In addition, the presence of a calcium-binding site, which increases the conformational stability and the binding affinity of TM to thrombin upon calcium coordination (*20*, *37*), imposes certain three-dimensional restrictions on the TM−thrombin interface. These data taken together may allow the definition of some essential details of the intermolecular contacts between thrombin and the fifth and sixth EGF-like domains of TM (TMEGF56). We therefore constructed a model of TMEGF456 docked to the exosite I of thrombin through a superposition of the C-loop of TMEGF5 on the structure of the hTM409−426 peptide in complex with thrombin (*18*). The molecular complex was optimized by energy minimization with the use of NOE and consensus calcium-binding site distance constraints (*35*) for a TM fragment encompassing the C-terminal peptide of TMEGF5 (*18*) and the hTM422−449 peptide. In some modeling runs we varied the initial position of the hTM422−449 fragment by turning the B-loop of TMEGF6 away from the consensus folding topology for EGF-like domains. This variation was achieved by modifying the φ and ψ dihedral angles of residues Cys427−Gly431, the junction between TMEGF5, and the B-loop of TMEGF6. After energy minimization, a portion of these nonconsensus starting conformations produced structures with significant NOE violations and without interaction contacts between the B-loop and the thrombin surface. The rest of the structures converged to a unique three-dimensional fold similar to a consensus structure of a calcium-binding EGF-like protein domain.

The model of the thrombin−TMEGF456 complex is shown in Figure 6, emphasizing only the peptide fragment, which directly participates in binding, or the C-terminal subdomain of TMEGF5 and the N-terminal subdomain of TMEGF6. Very interestingly, the peptide fragment corresponding to the β-hairpin of hTM422−449 comes into close contact with thrombin but only through the second strand of the hairpin, or residues Thr443−Ile447. The first strand of the hairpin, or residues Val436−Leu440, mostly faces away from the thrombin, presumably into the solvent. The interacting strand is located close to residues Leu108−

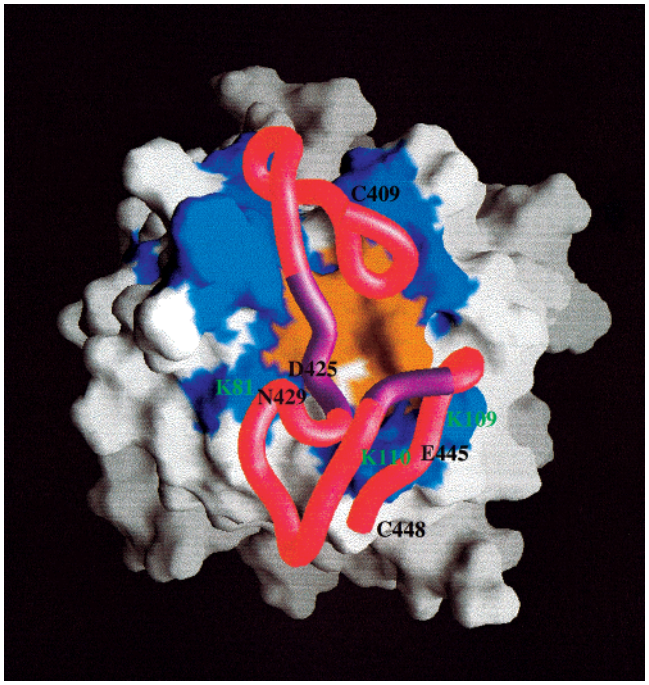

FIGURE 6: Three-dimensional model of part of the thrombin−thrombomodulin binding interface. Thrombin surface residues implicated in interaction with TM are colored in blue for the charged residues (*40*) and in brown for the hydrophobic residues. The C-loop of TMEGF5 and the N-terminal domain of TMEGF6 (residues 408−448 of TM) are represented as a continuous tube. Residues involved in calcium binding are shown in purple and the rest of the residues in red. Charged residues on the thrombin surface, which are spatially close to TMEGF6, are indicated by their sequence locations.

Lys110 of thrombin. In addition, residues Asp425 and Asn429 of TMEGF6 appear to be close to residue Lys81 of thrombin. It is therefore possible that the side chains of residues Lys109 and Lys110 of thrombin make electrostatic interactions with Glu445 of TM, while Lys81 interacts with one of the side-chain carboxyl groups of Asp425 and/or with the backbone carbonyl group of Asn429 of TM.

DISCUSSION

A 28-residue peptide encompassing the N-terminal subdomain of the sixth EGF-like repeat of human thrombomodulin plus the bridging residues connecting the fifth and the sixth EGF-like domains exhibits differential resonance perturbations and transferred NOEs in the presence of thrombin. This peptide is structurally reinforced by two disulfide bonds connected in a [1−3, 2−4] fashion, and it is shown to bind to calcium specifically (*20*), in agreement with other studies determining the location and the role of calcium binding sites in TM (*37*). The residues most affected by thrombin binding are located in the central β-hairpin, or B-loop, of a consensus EGF-like structural module. Formation of the β-hairpin upon binding is supported by transferred NOEs bringing the two strands together and identifying a type I β-turn. We demonstrated previously that calcium binding to the free peptide increases the tendency of the same residues in hTM422−449 to form β-sheet conformations (*20*). Light et al. also showed that occupancy of the calcium-binding site on human TM has a profound effect on the energetics of binding to thrombin and increases the β-sheet content of TMEGF456 (*37*).

A short cyclic peptide derived from the β-hairpin region of hTM422−449, or hTM436−447, also shows interactions with thrombin, as evidenced by NMR signal perturbations. It does not, however, inhibit fibrinogen clotting even at millimolar concentrations. The lack of inhibition does not necessarily mean the absence of specific binding, since thrombomodulin and fibrinogen binding sites appear to overlap only partially (*38*−*40*). This peptide binding appears to be also sequence-specific, since no binding was detected for highly homologous peptides of the same length. These results are in agreement with the competition binding studies of a series of peptides derived from TMEGF56 (*11*) and TMEGF456 (*12*). Two peptides corresponding to the Glu408−Glu426 and Pro441−Ala455 sequences were shown to be the best competitors for thrombin binding to thrombomodulin, with affinities of 85 and 117 μM, respectively (*11*). The first peptide, or Glu408−Glu426, corresponding to the C-terminal subdomain of TMEGF5, was also shown to be a potent inhibitor of fibrinogen clotting and protein C activation (*12*). The Pro441−Ala455 peptide spans the second and third loops of TMEGF6, and peptides from this region of TMEGF6 were all weak inhibitors of fibrinogen clotting and protein C activation (*12*). These data taken together suggest that the sixth EGF-like domain of TM directly participates in thrombin binding through the central B-loop region. More importantly, it appears that while the peptides derived from the fifth repeat of TM interact predominantly with the fibrinogen recognition site (or exosite I) (*16*, *18*), the sixth EGF-like repeat of TM may bind to a site outside of and around the exosite I of thrombin, as also proposed previously (*11*).

The distance constraints derived from the transferred NOE experiments and the consensus calcium-binding site generate a local fold of the thrombomodulin fragment, which is close to that expected for an EGF-like protein domain. When these constraints were utilized in a docking procedure, we obtained an approximate model for the spatial arrangement of TMEGF56 in the anion-binding exosite I of thrombin. This structure model identifies another interaction interface between thrombin and the sixth EGF-like domain of TM, involving residues Thr443−Ile447 of TM and Lys109−Val112 of thrombin. This modeling result is consistent with the differential proton resonance perturbations observed for short and cyclic hTM436−447 peptide, in which residues Thr443, Phe444, Cys446, and Ile447 are the most affected upon thrombin titration. Accordingly, the most prominent thrombin-induced resonance perturbations for the 28-residue peptide hTM422−449 are for residues Thr443, Ile447, and Ser448.

Our current model of TM interaction with human thrombin (Figure 6) fits well with the functional mapping of the interfacial residues of thrombin with TM (*39*, *40*). In addition to the amino acid residues implicated in the formation of the binding interface between the C-loop of TMEGF5 and thrombin, Hall et al. identified Lys81 and Lys109 as TM-binding residues utilizing a site-directed mutagenesis strategy (*40*). The effect of the Lys110Ala substitution is somewhat smaller than that of Lys109Ala, but its involvement in thrombomodulin binding cannot be ruled out. These residues are distant from the anionic C-loop of TMEGF5 (*16*, *18*), and their interaction with TMEGF6 might explain the reduced effects on protein C activation obtained with the corresponding thrombin mutants. The structural model of the TMEGF56−thrombin complex (Figure 6) also provides a rationalization for the functional roles of TMEGF5 and TMEGF6 identified using domain-deletion mutants of intact thrombomodulin (*11*). In other words, the TMEGF5 domain of TM, especially its C-terminal region from residues Cys409 to Glu426 appears to be the major anchor site between thrombin and TM, while additional interactions conferred by TMEGF6 serve to enhance the affinity of the TM−thrombin complex. In conclusion, the data presented in this study suggest a mode of interaction between thrombomodulin and thrombin, whereby the sixth EGF-like domain of thrombomodulin directly participates in binding rather than simply modulates the binding of the fifth EGF-like domain. The three-dimensional model of the TMEGF56−thrombin complex is consistent with the data obtained with model peptides *(11*, *12*, *20*, and the current study) and on the mapping of thrombin residues involved in the interaction with TM and in the activation of protein C (*40*).

During the review of this paper, a crystal structure of human α-thrombin in complex with TMEGF456 was reported (*41*). The crystal structure reveals that TM indeed utilizes mostly the C-terminal subdomain of TMEGF5 and part of TMEGF6 for binding to thrombin. Residues Cys409−Glu426 in the TMEGF456−thrombin complex adopt the canonical EGF-like backbone folding as shown by NMR studies (*17*, *18*, and Figure 6*)*, instead of the altered conformation defined by a previous X-ray study (*16*). The key contacts between TMEGF5 and thrombin are hydrophobic interactions between the side chains of both Ile414 and Ile424 and a hydrophobic pocket created by thrombin residues Phe34, Leu65, Tyr76, and Ile82, also in agreement with earlier predictions based on NMR results and docking studies (*18*). Consistent with the new X-ray structure (*41*), we found that the Glu428−Cys433 and His438−Ile447 sequence segments are partially structured upon binding of hTM422−449 to thrombin. The side chain of Phe444 forms close contacts with Asn439, Leu440, and Gly442, thus contributing to the stability of the central β-hairpin in the hTM422−449 fragment (Figure 4). However, our results suggest the presence of interactions between thrombin and the second strand of the central β-hairpin in TMEGF6 (Figure 6). This interaction is not observed in the crystal structure, while instead a single salt bridge between side chains of Lys110 of thrombin and Asp461 of TM is reported. It is possible that these structural differences can be explained by the difference in the length of the TM fragments used and/or by the use of apo- instead of calcium-bound peptides in the NMR studies. It is also possible that dynamic motions for the sixth EGF-like domain in solution impart different orientation(s) of TMEGF6 in complex with thrombin, as TMEGF6 is only partially structured even in the crystal state (*41*). Regardless, the definition of specific interactions between thrombin and a minimal fragment of the sixth EGF-like domain of human TM provides a further understanding of the nature of the binding contacts in the TM−thrombin complex and may lead to new avenues for the discovery of more effective modulators of blood coagulation.

ACKNOWLEDGMENT

We are grateful to Dr. Ping Xu for acquiring the NMR data on the 800 MHz NMR spectrometer.

REFERENCES

1. Engel, J. (1989) *FEBS Lett. 251*, 1−7.
2. Campbell, I. D., and Bork, P. (1993) *Curr. Opin. Struct. Biol. 3*, 385−392.
3. Lin, S. L., and Nussinov, R. (1995) *Nat. Struct. Biol. 2*, 835−837.
4. Harrison, P. M., and Sternberg, M. J. E. (1996) *J. Mol. Biol. 264*, 603−623.
5. Tsiang, M., Lentz, S. R., Dittman, W. A., Wen, D., Scarpati, E. M., and Sadler, J. E. (1990) *Biochemistry 29*, 10602−10612.
6. Esmon, C. T. (1989) *J. Biol. Chem. 264*, 4743−4746.
7. Stearns, D. J., Kurosawa, S., and Esmon, C. T. (1989) *J. Biol. Chem. 264*, 3352−3356.
8. Zushi, M., Gomi, K., Yamamoto, S., Maruyama, I., Hayashi, T., and Suzuki, K. (1989) *J. Biol. Chem. 264*, 10351−10353.
9. Kurosawa, S., Stearns, D. J., Jackson, K. W., and Esmon, C. T. (1988) *J. Biol. Chem. 263*, 5993−5996.
10. Nagashima, M., Lundh, E., Leonard, J. C., Morser, J., and Parkinson, J. F. (1993*) J. Biol. Chem. 268*, 2888−2892.
11. Tsiang, M., Lentz, S. R., and Sadler, J. E. (1992) *J. Biol. Chem. 267*, 6164−6170.
12. Lougheed, J. C., Bowman, C. L., Meininger, D. P., and Komives, E. A. (1995*) Protein Sci. 4*, 773−780.
13. Meininger, D. P., Hunter, M. J., and Komives, E. A. (1995) *Protein Sci. 4*, 1683−1695.
14. Benitez, B. A. S., Hunter, M., Meininger, D. P., and Komives, E. A. (1997) *J. Mol. Biol. 273*, 913−926.
15. White, C. E., Hunter, M. J., Meininger, D. P., Garrod, S., and Komives, E. A. (1996*) Proc. Natl. Acad. Sci. U.S.A. 93*, 10177−10182.
16. Mathews, I. I., Padmanabhan, K. P., Tulinsky, A., and Sadler, J. E. (1994) *Biochemistry 33*, 13547−13552.
17. Srinivasan, J., Hu, S., Hrabal, R., Zhu, Y., Komives, E. A., and Ni, F. (1994) *Biochemistry 33*, 13553−13560.
18. Hrabal, R., Komives, E. A., and Ni, F. (1996) *Protein Sci. 5*, 195−203.
19. White, C. E., Hunter, M. J., Meininger, D. P., White, L. R., and Komives, E. A. (1995) *Protein Eng. 8*, 1177−1187.
20. Tolkatchev, D., and Ni, F. (1998) *Biochemistry 37*, 9091−9100.
21. Handford, P. A., Baron, M., Mayhew, M., Willis, A., Beesley, T., Brownlee, G. G., and Campbell, I. D. (1990) *EMBO J. 9*, 475−480.
22. Stenflo, J., Öhlin, A.-K., Owen, W. G., and Schneider, W. J. (1988) *J. Biol. Chem. 263*, 21−24.
23. Ni, F. (1994) *Prog. NMR Spectrosc. 26*, 517−606.
24. Ni, F., Konishi, Y., and Scheraga, H. A. (1990) *Biochemistry 29*, 4479−4489.
25. Braunschweiler, L., and Ernst, R. R. (1983) *J. Magn. Reson. 53*, 521−528.
26. Lippens, G., Dhalluin, C., and Wieruszeski, J.-M. (1995) *J. Biomol. NMR 5*, 327−331.
27. Piotto, M., Saudek, V., and Sklenar, V. (1992) *J. Biomol. NMR 2*, 661−665.
28. Bax, A., and Davis, D. G. (1985) *J. Magn. Reson. 65*, 335−360.
29. Kjaer, M., Andersen, K. V., and Poulsen, F. M. (1994) *Methods Enzymol. 29*, 288−318.
30. Ni, F., Meinwald, Y. C., Vasquez, M., and Scheraga, H. A. (1989) *Biochemistry 28*, 3094−3105.
31. Brunger, A. T. (1992) *X-PLOR (Version 3.1): A System for X-ray Crystallography and NMR*, Yale University Press, New Haven and London.
32. Vasquez, M., and Scheraga, H. A. (1988) *J. Biomol. Struct. Dyn. 5*, 705−755.
33. Ni, F., Konishi, Y., and Scheraga, H. A. (1990) *Biochemistry 29*, 4479−4489.
34. Ni, F., Zhu, Y., and Scheraga, H. A. (1995) *J. Mol. Biol. 252*, 656−671.
35. Rao, Z., Handford, P., Mayhew, M., Knott, V., Brownlee, G. G., and Stuart, D. (1995) *Cell 82*, 131−141.
36. Rizo, J., and Gierasch, L. M. (1992) *Annu. Rev. Biochem. 61*, 387−418.
37. Light, D. R., Glaser, C. B., Betts, M., Blasko, E., Campbell, E., Clarke, J. H., McCaman, M., McLean, K., Nagashima, M., Parkinson, J. F., Rumennik, G., Young, T., and Morser, J. (1999) *Eur. J. Biochem. 262*, 522−533.
38. Wu, Q. Y., Sheehan, J. P., Tsiang, M., Lentz, S. R., Birktoft, J. J., and Sadler, J. E. (1991) *Proc. Natl. Acad. Sci. U.S.A. 88*, 6775−6779.
39. Tsiang, M., Jain, A. K., Dunn, K. E., Rojas, M. E., Leung, L. L. K., and Gibbs, C. S. (1995) *J. Biol. Chem. 270*, 16854−16863.
40. Hall, S. W., Nagashima, M., Zhao, L., Morser, J., and Leung, L. L. K. (1999) *J. Biol. Chem. 274*, 25510−25516.
41. Fuentes-Prior, P., Iwanaga, Y., Huber, R., Pagila, R., Rumennik, G., Seto, M., Morser, J., Light, D. R., and Bode, W. (2000) *Nature 404*, 518−525.

BI000715E